Analysis of Optimal Deployment Strategy for Large Deployable Tensegrity Space Antennas

Muhao Chen[1] , Aguinaldo Fraddosio[2] , Andrea Micheletti[3] ,
Gaetano Pavone[2(✉)] , Mario Daniele Piccioni[2] , and Robert E. Skelton[1]

[1] Department of Aerospace Engineering, Texas A&M University, College Station,
TX, USA
{muhaochen,bobskelton}@tamu.edu

[2] Department of Architecture, Construction and Design, Polytechnic University of
Bari, Bari, Italy
{aguinaldo.fraddosio,gaetano.pavone,mariodaniele.piccioni}@poliba.it

[3] Department of Civil and Computer Science Engineering, University of Rome Tor
Vergata, Rome, Italy
micheletti@ing.uniroma2.it

Abstract. This study introduces an integrated approach that merges the design of structure and control to study the deployment strategies for tensegrity structures, particularly in the context of space antennas. First, we establish a nonlinear shape control law for clustered tensegrity structures, the solution turns out to solve a constraint linear algebra equation. Leveraging the symmetric nature of the antenna structure, we designate active actuators for the top and bottom cables of the space antenna while considering the remaining cables as passive. To further reduce the number of actuators required, we employ various clustering strategies for the active actuating cables. Results show that the deployment from the initial state to the predetermined targets is successfully guided by the proposed control law through clustering active cables using different actuation strategies. It is significant to note, however, that the energy cost escalates as more cables are clustered into the deployable antenna structures. In the context of space applications, this scenario emphasizes structure design and control are not independent problems. These insights also offer extensive relevance and can be extrapolated to different deployable tensegrity structures and robotic systems.

Keywords: Space Antenna · Deployable Structure · Tensegrity Structure · Deployment strategy · Integrated Structure and Control Design

1 Introduction

In light of the substantial expenses associated with launching and the constrained size of rocket tanks, the aerospace industry is continuously pursuing lightweight

and deployable alternatives [2]. Recently, the European Space Agency (ESA) commissioned a study to explore breakthrough architectural concepts that offer superior reliability for the deployment of large systems. According to a previous study [7], the application of the new tensegrity-type architectural concept to large space antenna reflectors has shown that it achieves reliability by significantly reducing the number of articulated joints when compared to non-tensegrity architectures. Ganga et al. analyzed the overall feasibility of the deployable system, as well as its design, stiffness, deployment repeatability, and geometric precision by experiments [7]. However, the optimal deployment strategy in terms of structure design and control is still an open question.

Tensegrity structures offer a plethora of cables, which can provide a wide range of options for actuators [4,6]. However, the availability of numerous cables can pose challenges in their practical application [5], such as increased costs for actuators, difficulties in their placement, complicated control, and higher energy requirements. To address this issue, it is necessary to select only a subset of cables as actuators while ensuring that the desired control performance is achieved.

Skelton et al. proposed a systematic design method for sensors and actuators in structural control to minimize the cost of instrumentation [11]. Chen et al. presented the energy-efficient cable-actuation strategy for tensegrity structures [1]. Feng et al. compared the control energy and optimal dynamic performance of clustered tensegrity structures with different actuator placements for clustered cables and struts [12]. Ma et al. presented the dynamics and control law to clustered tensegrity structures [9]. However, most of the research on actuator selection has been conducted on linear systems, whereas tensegrity is a nonlinear system. Limited studies have been conducted on finding energy-efficient control laws with an optimal number of actuators.

This paper presents an energy-effective method for achieving nonlinear shape control in tensegrity structures. The subsequent sections are organized as follows: Sect. 2 introduces the design of deployable tensegrity space antennas. Section 3 outlines the shape control equation for tensegrity structures, derived from nonlinear dynamics formulations, utilizing cable forces as variables with imposed constraints. We also provide solutions to the shape control equation, along with clustering actuation strategies and minimal control energy considerations. In Sect. 4, numerical examples are presented to demonstrate the accuracy and efficiency of the control law and optimal clustering strategy. Finally, Sect. 5 summarizes the study's conclusions.

2   Design of Deployable Tensegrity Space Antennas

2.1   The Tensegrity Antenna Topology

Definition 1 (The Tensegrity Antenna). *Figure. 1 illustrates the structural topology of the deployable tensegrity antenna. The complexity q of the structure is defined by the number of X units in the structure. Figure 2 displays the structure with varying complexities.*
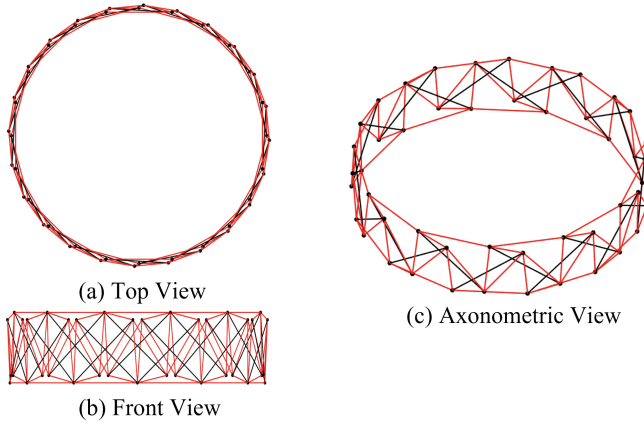
(a) Top View

(c) Axonometric View

(b) Front View

Fig. 1. A tensegrity ring: (a) top, (b) front, and (c) axonometric views with structure complexity of $q = 12$. The thick black lines are bars, and the thin red lines are cables.
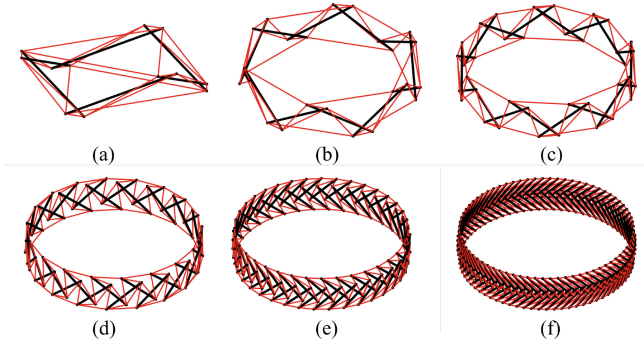

(a)   (b)   (c)

(d)   (e)   (f)

Fig. 2. The tensegrity antenna with different complexities: (a) $q = 3$, (b) $q = 6$, (c) $q = 9$, (d) $q = 12$, (e) $q = 36$, and (f) $q = 72$.

By shrinking the top and bottom cables simultaneously, we can have a deployable antenna. The structure deployment configurations are shown in Fig. 3.

3 Nonlinear Shape Control Law

3.1 Nonlinear Equations of Motion of Full-Order Model

Definition 2 (Nodal Coordinates). *The nodal coordinate vector $\boldsymbol{n} \in \mathbb{R}^{3n_n}$ and matrix $\boldsymbol{N} \in \mathbb{R}^{3 \times n_n}$ in a tensegrity system are:*

$$\boldsymbol{n} = \begin{bmatrix} \boldsymbol{n}_1^T \ \boldsymbol{n}_2^T \ \cdots \ \boldsymbol{n}_{n_n}^T \end{bmatrix}^T, \tag{1}$$

where $\boldsymbol{n}_i = \begin{bmatrix} x_i \ y_i \ z_i \end{bmatrix}^T \in \mathbb{R}^3$ is the x-, y-, and z-coordinates of the ith (i = $1, 2, \cdots, n_n$) node, and n_n is the total number of nodes.
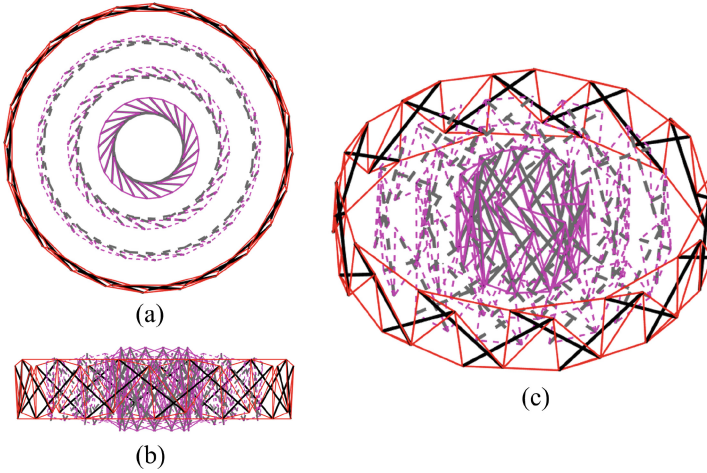
Fig. 3. Deployed, transient, and folded configurations: (a) top view, (b) front view, and (c) axonometric view. The diameters of the circles depicted in the views are 12 m, 9 m, 6 m, and 3 m, arranged from the outermost to the innermost circle. The initial state is represented by the 12 m diameter circle, with black and red lines denoting the bars and cables, respectively. The transient states are illustrated by the 9 m and 6 m diameter circles, where dotted grey and magenta lines are used to depict the bars and cables, respectively. Finally, the target state is portrayed by the 3 m diameter circle, with grey and magenta lines representing the bars and cables, respectively.

Definition 3 (Connectivity Matrices). *The connectivity matrices C_s and C_b describe the overall pattern of connections between the cables and bars in a tensegrity system, respectively. The total connectivity matrix C is obtained by concatenating C_s and C_b and has dimensions $\mathbb{R}^{n_e \times n_n}$, where $n_e = n_s + n_b$ is the total number of structural elements. Each row of C corresponds to an element $m = 1, 2, \cdots, n_e$ and is represented by the vector C_m. The i-th entry of C_m indicates the connection between the two nodes associated with the element m. Specifically, the i-th entry of C_m is defined as follows:*

$$C_{mi} = \begin{cases} -1, & i = j \\ 1, & i = k \\ 0, & otherwise \end{cases}, \tag{2}$$

where $j = 1, 2, \cdots, n_n$ and $k = 1, 2, \cdots, n_n$.

Theorem 1 (Tensegrity Nonlinear Dynamics). *The tensegrity dynamics with constraints is given by:*

$$E_a^T (M\ddot{n} + D\dot{n} + Kn) = E_a^T (f_{ex} - g), \tag{3}$$

where

$$M = \frac{1}{6}(|C|^T \hat{m}|C| + \lfloor |C|^T \hat{m}|C| \rfloor) \otimes I_3, \tag{4}$$

$$K = (C^T \hat{x} C) \otimes I_3, \tag{5}$$

$$g = \frac{g}{2}(|C|^T m) \otimes \begin{bmatrix} 0 & 0 & 1 \end{bmatrix}^T, \tag{6}$$

where $M \in \mathbb{R}^{3n_n \times 3n_n}$, $D \in \mathbb{R}^{3n_n \times 3n_n}$, and $K \in \mathbb{R}^{3n_n \times 3n_n}$ are mass, damping, and stiffness matrices, $\hat{\bullet}$ operator converts the vector into a diagonal matrix, $|V|$ gets the absolute value of each element of the matrix V, and $\lfloor V \rfloor$ sets all the off-diagonal elements of a square matrix to zero. $x \in \mathbb{R}^{n_e}$ is the force density (force per unit length) vector of structure members, $f_{ex} \in \mathbb{R}^{3n_n}$ is external forces on the structure nodes, and g is gravity vector (g is the gravity constant, e.g., $g = 9.81\,m/s^2$ for earth gravity). $E_a \in \mathbb{R}^{3n_n \times n_a}$ (n_a are the number of free nodes) is an orthonormal matrix to extract free nodes n_a from nodal vector n, which satisfies $E_a(:,i) = I_{3n}(:,a_i) \in \mathbb{R}^{3n_n \times n_a}$ and $n_a = E_a^T n$. The value a_i in vector $a = \begin{bmatrix} a_1 & a_2 & \cdots & a_{n_a} \end{bmatrix}^T \in \mathbb{R}^{n_a}$ are the indices of the free nodes in the nodal coordinate vector n. Similarly, vector $b = \begin{bmatrix} b_1 & b_2 & \cdots & b_{n_b} \end{bmatrix}^T \in \mathbb{R}^{n_b}$ are the indices of constrained entries in the nodal coordinate vector n. $E_b(:,i) = I_{3n}(:,b_i) \in \mathbb{R}^{3n_n \times n_b}$ is an orthonormal matrix to abstract constrained nodes n_b from nodal vector n and $n_b = E_b^T n$, The sum of the number of free and fixed nodes is the total number of nodes, and we have $n_a + n_b = 3n_n$.

Proof. Theorem 1 can be derived using the Lagrangian method, and the details are given in [10] and software package [8].

We also provide the statics equations since this part will be used in the later control equations.

Corollary 1 (Tensegrity Statics). *The tensegrity statics with constraints has three equivalent forms:*

$$E_a^T K n = E_a^T A_{1c} x_c = E_a^T A_{2c} t_c = E_a^T (f_{ex} - g), \tag{7}$$

where

$$A_{1c} = A_{2c} \hat{l}_c = (C^T \otimes I_3)\, b.d.(H) \hat{l}^{-1} S^T \hat{l}_c. \tag{8}$$

Proof. By neglecting the time derivatives in Theorem 1, we can have $E_a^T K n = E_a^T (f_{ex} - g)$. From Eq. (5), one can get $K n = A_{1c} x_c = A_{2c} t_c$.

3.2 Shape Control Law

Definition 4 (Shape Objectives). *The error between the current position of the structure to the control target is defined as:*

$$e = n_c - \bar{n}_c, \tag{9}$$

where $\boldsymbol{n}_c$ is the nodes of interest to control, $\bar{\boldsymbol{n}}_c$ is the morphing objective. Since the nodal coordinate of interest $\boldsymbol{n}_c$ is extracted from the free nodal coordinate $\boldsymbol{n}_a$, we have $\boldsymbol{n}_c = \boldsymbol{E}_c^T \boldsymbol{n}_a$, where $\boldsymbol{E}_c$ is the index matrix.

Definition 5 (Active and Passive Members). *The active and passive cables are defined as the structure members who actively and passively change their length, satisfying $n_s = n_{s,act} + n_{s,pas}$, where $n_{s,act}$ and $n_{s,pas}$ are the number of active and passive cables, respectively. The force vectors of the active and passive members can be written as follows:*

$$\boldsymbol{t}_{c_{act}} = \boldsymbol{E}_{act}^T \boldsymbol{t}_c, \; \boldsymbol{t}_{c_{pas}} = \boldsymbol{E}_{pas}^T \boldsymbol{t}_c, \tag{10}$$

where $\boldsymbol{E}_{act}$ and $\boldsymbol{E}_{pas}$ are index matrices to separate all the structure members. Since $\begin{bmatrix} \boldsymbol{E}_{act} & \boldsymbol{E}_{pas} \end{bmatrix}$ is an orthogonal matrix, we have the following equation:

$$\boldsymbol{t}_c = \begin{bmatrix} \boldsymbol{E}_{act}^T \\ \boldsymbol{E}_{pas}^T \end{bmatrix}^{-1} \begin{bmatrix} \boldsymbol{t}_{c_{act}} \\ \boldsymbol{t}_{c_{pas}} \end{bmatrix} = \begin{bmatrix} \boldsymbol{E}_{act} & \boldsymbol{E}_{pas} \end{bmatrix} \begin{bmatrix} \boldsymbol{t}_{c_{act}} \\ \boldsymbol{t}_{c_{pas}} \end{bmatrix}. \tag{11}$$

Theorem 2 (Nonlinear Shape Control). *The nonlinear shape control of the tensegrity structure is equivalent to solving the following linear algebra equation:*

$$\boldsymbol{\mu} - \boldsymbol{\Gamma}_{pas} \boldsymbol{t}_{c_{pas}} = \boldsymbol{\Gamma}_{act} \boldsymbol{t}_{c_{act}}, \tag{12}$$

where $\boldsymbol{\mu}$, $\boldsymbol{\Gamma}_{act}$, and $\boldsymbol{\Gamma}_{pas}$ are:

$$\boldsymbol{\mu} = \boldsymbol{E}_c^T \boldsymbol{M}_{aa}^{-1} \boldsymbol{E}_a^T (\boldsymbol{f}_{ex} - \boldsymbol{g} - \boldsymbol{M} \boldsymbol{E}_b \ddot{\boldsymbol{n}}_b - \boldsymbol{D}\dot{\boldsymbol{n}})$$
$$- \ddot{\bar{\boldsymbol{n}}}_c + \boldsymbol{\psi}(\boldsymbol{E}_c^T \dot{\boldsymbol{n}}_a - \dot{\bar{\boldsymbol{n}}}_c) + \boldsymbol{\phi}(\boldsymbol{E}_c^T \boldsymbol{n}_a - \bar{\boldsymbol{n}}_c), \tag{13}$$

$$\boldsymbol{\Gamma}_{act} = \boldsymbol{E}_c^T \boldsymbol{M}_{aa}^{-1} \boldsymbol{E}_a^T \boldsymbol{A}_{2c} \boldsymbol{E}_{act}, \tag{14}$$

$$\boldsymbol{\Gamma}_{pas} = \boldsymbol{E}_c^T \boldsymbol{M}_{aa}^{-1} \boldsymbol{E}_a^T \boldsymbol{A}_{2c} \boldsymbol{E}_{pas}. \tag{15}$$

Proof. When the nodes of interest reach their targets, the error vector $\boldsymbol{e}$ and its time derivatives should all go to zero. This goal can be expressed as follows [3]:

$$\ddot{\boldsymbol{e}} + \boldsymbol{\psi}\dot{\boldsymbol{e}} + \boldsymbol{\phi}\boldsymbol{e} = \boldsymbol{0}, \tag{16}$$

where $\boldsymbol{\psi}$ and $\boldsymbol{\phi}$ are tune matrices that can adjust the time response of the morphing process. Since $\boldsymbol{E}_c$ is given constants, the time derivatives of the error vector in Eq. (9) are:

$$\dot{\boldsymbol{e}} = \dot{\boldsymbol{n}}_c - \dot{\bar{\boldsymbol{n}}}_c, \; \ddot{\boldsymbol{e}} = \ddot{\boldsymbol{n}}_c - \ddot{\bar{\boldsymbol{n}}}_c. \tag{17}$$

Substitute Eqs. (3) and (9) into Eq. (16), we have:

$$\boldsymbol{E}_c^T \boldsymbol{M}_{aa}^{-1} \boldsymbol{E}_a^T (\boldsymbol{f}_{ex} - \boldsymbol{g} - \boldsymbol{M} \boldsymbol{E}_b \ddot{\boldsymbol{n}}_b - \boldsymbol{D}\dot{\boldsymbol{n}} - \boldsymbol{K}\boldsymbol{n})$$
$$- \ddot{\bar{\boldsymbol{n}}}_c + \boldsymbol{\psi}(\boldsymbol{E}_c^T \dot{\boldsymbol{n}}_a - \dot{\bar{\boldsymbol{n}}}_c) + \boldsymbol{\phi}(\boldsymbol{E}_c^T \boldsymbol{n}_a - \bar{\boldsymbol{n}}_c) = \boldsymbol{0}. \tag{18}$$

Substitute Eqs. (8) and (11) into Eq. (18), one can have a linear algebra Eqs. (12)–(15).

3.3   Solving for Control Variable

The only unknown variable in Eq. (12) is $\boldsymbol{t}_{c_{act}}$. In most cases, people use cables to control the tensegrity structure, so let us use cable as the control variable as an example. Since cables cannot take compression, and if they do, we should substitute the force to zero, we must add the constraint to this unknown variable $\boldsymbol{t}_{c_{act}} \geq \boldsymbol{0}$. Moreover, the cables should never exceed their yield strength, which can be calculated by the $\sigma_s \boldsymbol{A}_c$. Thus, the problem of solving Eq. (12) becomes a linear algebra problem with inequality constraints.

Theorem 3 (Shape Control Solution). *The solution to Theorem 3.2 is as the following:*

$$\begin{cases} \underset{\boldsymbol{t}_{c_{act}}}{Solve} & \boldsymbol{\Gamma}_{act}\boldsymbol{t}_{c_{act}} = \boldsymbol{\mu} - \boldsymbol{\Gamma}_{pas}\boldsymbol{t}_{c_{pas}} \\ s.t. & \boldsymbol{0} \leq \boldsymbol{t}_{c_{act}} \leq \sigma_s \boldsymbol{A}_c \end{cases}. \tag{19}$$

The resolution of Theorem 3 relies on the characteristics of $\boldsymbol{\Gamma}_{act}$. One favorable feature of tensegrity structures is that they contain an abundant number of cables, resulting in $\boldsymbol{\Gamma}_{act}$ being a matrix with a complete column rank, thereby making at least one solution typically exist. It is worth mentioning that an analytical solution could exist, such as finding solutions from the positive span space in the first equation. However, for different structures, a solution cannot always be guaranteed, but a least square one is always possible, $\underset{\boldsymbol{t}_{c_{act}}}{\min}||\boldsymbol{\mu} - \boldsymbol{\Gamma}_{pas}\boldsymbol{t}_{c_{pas}} - \boldsymbol{\Gamma}_{act}\boldsymbol{t}_{c_{act}}||^2$. We should point out that the least square solution can be arbitrarily bad. Thus, one has to be careful in choosing the target points, control speed, and materials.

3.4   Deployment Strategy Design

In an effort to optimize both the manufacturing process and deployment strategy, we have thoroughly taken advantage of the symmetrical properties of the structure. Specifically, we choose passive cables for the side cables and active cables for the top and bottom cables.

Definition 6 (Clustering Actuation Strategy). *The structure clustering strategy is shown in Fig. 4, where we use the complexity of $q = 12$ as an example to illustrate the idea.*

Definition 7 (The Energy Cost). *The total control energy of the system can be computed as follows:*

$$E = \sum_{i=1}^{k} \Delta\boldsymbol{l}_{c_{act},i}^{T}\boldsymbol{t}_{c_{act},i}, \tag{20}$$

where $\Delta\boldsymbol{l}_{c_{act},i}$ represents the change in length of the active members at the ith step, $\boldsymbol{t}_{c_{act},i}$ denotes the member force in the active members at the ith step, and k is the total time steps of the active actuation process.
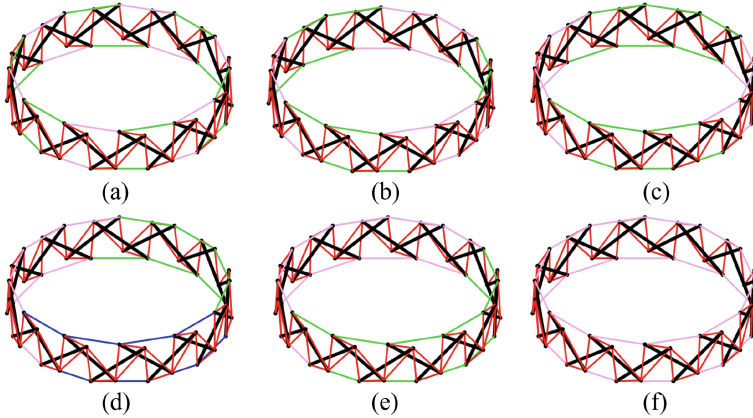
Fig. 4. The clustering strategies involve individual passive cables represented by red cables, as well as active cables found in the top and bottom cables. Within these top and bottom cables, six clustering strategies are employed: (a) non-clustered cables, (b) clustering of every two adjacent cables, (c) clustering of every three adjacent cables, (d) clustering of every four adjacent cables, (e) clustering of every six adjacent cables, and (f) clustering of all twelve adjacent cables.

4   Numerical Results

To demonstrate the proposed method, we choose the antenna complexity to be $q = 12$, as shown in Figs. 1 and 3. The diameter of the ring is 12 m, and the height of ring H is 2.6 m. The end module's height is 2.5m. The damping coefficient is 0.1. The time step is 0.0001 s, and the total simulation time is 20 s. The target node positions are computed from the static deployment process by adjusting the inner ring diameter to be 3 m. The material properties are given in Table 1. In this study, we examine the six cases as shown in Fig. 4. We use the same setups for all six cases except for the clustering strategies. We choose the same control gains for the six cases.

Table 1. Material properties of the structure members.

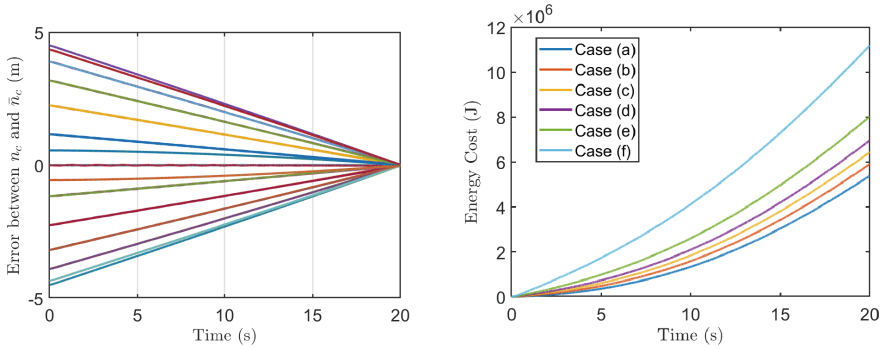| Properties	Bars	Passive Cables	Active Cables
Material	Steel	Aluminum	UHMWPE
Diameter	16 mm	4 mm	10 mm
Density	7,7870 kg/m^3	2,700 kg/m^3	970 kg/m^3
Young's Modulus	206 Gpa	60 Gpa	120 Gpa
Yield Strength	300 Mpa	110 Mpa	2.7 Gpa

Fig. 5. Left: The performance of control measured by the errors between the current position and the control targets of all the inner nodes of the structure. No significant difference was found between the six clustering strategies in Fig. 4. Right: The control energy cost for the six clustering strategies (a)-(f) in Fig. 4.

As evident from Fig. 5 (left), the control performance, measured by the errors between the current position and control targets, is roughly zero at the final simulation time for all six clustering strategies. This implies that the control law is effective in guiding the structure toward the final targets. However, as we cluster more cables, the energy cost is higher. For example, as shown in Fig. 5 (Right), the energy cost at the final state for the listed six cases are 5.3887×10^6 J, 5.9111×10^6 J, 6.4374×10^6 J, 6.9644×10^6 J, 8.0223×10^6 J, and 1.1183×10^7 J. That is, by clustering cables, one can use fewer actuators in the antenna structure, but the energy cost is higher. One can note that in case (f), where all twelve nearby cables are clustered, the energy consumption is 2.0752 times that of case (a), which involves non-clustered cables. However, this setup results in the saving of 11 actuators.

It is worth noting that energy resources in space applications, such as those derived from solar panels, are fairly restricted. Consequently, in such instances, there must be a careful equilibrium between energy consumption and the number of actuators used. This scenario underlines that, in the context of space applications, the design of the structure and its control are intertwined and should not be considered separate issues.

5   Conclusions

This paper presents an integrated approach that combines structure and control design to study the deployment strategy for tensegrity deployable structures, with a focus on space antennas. We derive a nonlinear shape control law for clustered tensegrity structures by solving a constraint linear algebra equation. The top and bottom cables are selected as active, while the remaining cables are passive. By clustering the active cables using different actuation strategies, the proposed control law effectively drives the structure from its initial configuration

to the desired targets. However, it is important to consider that the energy cost increases as more cables are clustered in deployable antenna structures. These findings have broad applicability and can be extended to other types of deployable tensegrity structures and robots.

References

1. Chen, M., Fraddosio, A., Micheletti, A., Pavone, G., Piccioni, M.D., Skelton, R.E.: Energy-efficient cable-actuation strategies of the v-expander tensegrity structure subjected to five shape changes. Mech. Res. Commun. **127**, 104026 (2023)
2. Chen, M., Goyal, R., Majji, M., Skelton, R.E.: Review of space habitat designs for long term space explorations. Prog. Aerosp. Sci. **122**, 100692 (2021)
3. Chen, M., Liu, J., Skelton, R.E.: Design and control of tensegrity morphing airfoils. Mech. Res. Commun. **103**, 103480 (2020)
4. Fraddosio, A., Marzano, S., Pavone, G., Piccioni, M.D.: Morphology and self-stress design of v-expander tensegrity cells. Compos. B Eng. **115**, 102–116 (2017)
5. Fraddosio, A., Pavone, G., Piccioni, M.D.: Minimal mass and self-stress analysis for innovative v-expander tensegrity cells. Compos. Struct. **209**, 754–774 (2019)
6. Fraddosio, A., Pavone, G., Piccioni, M.D.: A novel method for determining the feasible integral self-stress states for tensegrity structures. Curved Layered Struct. **8**(1), 70–88 (2021)
7. Ganga, P.L., Micheletti, A., Podio-Guidugli, P., Scolamiero, L., Tibert, G., Zolesi, V.: Tensegrity rings for deployable space antennas: concept, design, analysis, and prototype testing. Variational Analysis and Aerospace Engineering: Mathematical Challenges for the Aerospace of the Future, pp. 269–304 (2016)
8. Ma, S., Chen, M., Skelton, R.: TsgFEM: tensegrity finite element method. J. Open Source Softw. **7**(75), 3390 (2022)
9. Ma, S., Chen, M., Skelton, R.E.: Dynamics and control of clustered tensegrity systems. Eng. Struct. **264**, 114391 (2022)
10. Ma, S., Chen, M., Skelton, R.E.: Tensegrity system dynamics based on finite element method. Compos. Struct. **280**, 114838 (2022)
11. Skelton, R.E., Li, F.: Economic sensor/actuator selection and its application to flexible structure control. Smart Structures and Materials 2004: Modeling, Signal Processing, and Control (2004)
12. Xiaodong, F., Yaowen, O., Mohammad, S.M.: Energy-based comparative analysis of optimal active control schemes for clustered tensegrity structures. Struct. Control Health Monit. **25**(19) (2018)